

Water Worlds

We present the study of the thermal emission of five aquaplanets. As in the previous chapters, we study the physical characteristics of the planet, their influence on the climate, the global infrared emission, and the shape of the thermal light curve observed at different geometries. Because of the homogeneity of the surface, the variability of the signal is produced by the presence of clouds. We are interested in the influence of clouds on the retrieval of the rotation rate. We have used LMD Global Climate Model data of five aquaplanets with the same atmospheric composition as the Earth and we have modified the rotation rate and the tilt of the rotation axis. Section 6.1 is an introduction to this type of planets; Section 6.2 describes the general characteristics of the climate of aquaplanets and the results of our set of study; in Section 6.3, we compare the infrared light curves of non-synchronous and synchronous aquaplanets; in Section 6.4, we discuss the retrieval of the rotational period in planets without continents; Section 6.5 presents the longitudinal curves; and in Section 6.6, we give the conclusions of our study.

6.1 Introduction

Present oceans cover $\sim 71\%$ of the Earth surface, but some geological models show that continents could have been mostly immersed at the end of the Archaean eon (~ 2.5 Gyrs ago) with only a fractional area of $2 - 3\%$ of the Earth was emerged land (Flament et al., 2008). It is possible then that at a certain epoch the early Earth had been covered with water except for a little fraction of its surface emerged in the form of small islands (Belousova et al., 2010; Guitreau et al., 2012). Water worlds could be common within the circumstellar Habitable Zone (HZ). For this reason, it is interesting to study this type of planets. The amount of water on a terrestrial planet could vary considerably as it depends on the delivery of water from sources

outside the HZ. Using N-body simulations to reproduce the formation of the inner Solar system, and assuming that the fraction of water is $\sim 10\%$ in the outer main belt, Raymond et al. (2007) found that they typically form an Earth like planet within the HZ with 1-10 times the amount of water on Earth. According to the so-called "Grand Tack" model, the distribution of water in the main belt is tightly associated with the specific formation and orbital evolution of the giant planets of the Solar System (Walsh et al., 2012) and could vary from one planetary system to another. On the Earth, approximately half of the total amount of water constitutes the oceans, and the other half is held within the mantle. This distribution is not fully understood although some hypotheses have been proposed (Kasting & Holm, 1992) and could also be different on another planet. If we assume that this ratio and the bulk composition of the planet (0.1% of H_2O in mass) are constant, the fraction of emerged land would decrease for a more massive planet. Indeed, the mass-radius relationship is given by $R_P/R_\oplus = (M_P/M_\oplus)^{0.274}$ (Sotin et al., 2007), and thus the depth of the ocean would increase as $2.7 \text{ km} \times (M_P/M_\oplus)^{-0.274}$. On an Earth replica twice as massive as our planet, the ocean would therefore be 20% deeper while the highest mountain (that scale as gravity^{-1}) would be 20% lower.

However, planets of terrestrial mass may have a very different origin than the Earth and it is expected that some of them may consist in a much larger fraction of water. An ocean planet, as proposed by Kuchner (2003) and Léger et al. (2004), is an Earth-like planet ($\leq 10M_\oplus$) formed of cometary material in the outer cold regions. Afterwards, the body migrates into the Habitable Zone (HZ) where the ices melt into liquid water oceans that cover the surface. The formation of a water-rich planet ending in the HZ can also be triggered by the migration of giant planets (Raymond et al., 2006). Having lower density, the radius of an ocean-planet is larger and its gravity lower than in terrestrial analogues (Sotin et al., 2007; Adams et al., 2008). This property make this type of planets easier to detect by transit missions like CoRoT or Kepler (Selsis et al., 2007) and easier to study by spectrophotometry (JWST).

Planets covered by oceans with any or little emerged lands are thus an expected

Table 6.1. Planetary specifics

	Rotation period (sidereal days)	Obliquity (degrees)	Excentricity	Type of planet
Ete-1 ^a	1	23.44	0.0167	Earth-like
Ote-1 ^a	1	23.44	0.0167	Aquaplanet
O-1	1	0.00	0.000	Aquaplanet
O-10	10	0.00	0.000	Aquaplanet
Os-1	1	0.00	0.0000	Synchronous aquaplanet
Os-10	10	0.00	0.0000	Synchronous aquaplanet
Os-360	360	0.00	0.0000	Synchronous aquaplanet

^aValues of Earth (Ete-1) and Ote-1 (Chapter 5) are given for comparison.

result of planet formation and evolution. The Earth itself may have been mostly covered by water during half of its history (although neither the atmosphere nor the oceans had the same characteristics as present Earth). The discovery of extrasolar water worlds would open a new field of comparative planetology. Because of their homogeneity, this type of planets is interesting to study the interaction between the ocean and the atmospheric circulation. In addition, their environmental conditions will be valuable to examine the hydrothermal origin of life (Wächtershäuser, 1988, 1990).

6.2 Planetary characteristics

In addition to the stellar insolation, the energy budget of a planet and its climate depend on many factors, such as the atmospheric composition, surface characteristics, and the circulation of the atmosphere and ocean. On an Earth-like planet, the circulation modulates the temperature by directly transporting energy and setting the distribution of water vapor and clouds.

Table 6.2. Global parameters of radiation

	T_{eff}^a (K)	A	CRF (W/m ²)	g_N	T_S (K)	∇T_S^φ (K)	∇T_S^ϕ (K)	$\Delta\varphi_S^{max}$ (°E)	$\Delta\phi_S^{ice}$ (°lat)
Ete-1 ^b	255	0.30	-27.2	0.39	288	-	50-80	-	-
Ote-1 ^b	258	0.26	-28.7	0.41	294	-	54	-	75
O-1	257	0.27	-27.4	0.39	291	-	74	-	60
O-10	245	0.40	-31.3	0.33	270	-	75	-	45
Os-1	238	0.46	-20.6	0.23	254	22	96	15	50
Os-10	231	0.52	-15.5	0.09	237	65	84	15	60
Os-360	231	0.53	-15.5	0.09	236	66	66	0	60

Note. — Effective temperature T_{eff} , albedo A, cloud radiative forcing CRF, normalized greenhouse parameter g_N and surface temperature T_S (Section 2.2). ∇T_S^φ and ∇T_S^ϕ are the zonal and meridional temperature gradients. $\Delta\varphi_S^{max}$ is the eastward shift of the surface temperature maximum in degrees. $\Delta\phi_S^{ice}$ is the maximum extension of the ice caps in latitude at the longitude of the substellar point.

^aThe temperature uncertainty is $\pm 5 \cdot 10^{-4} K$, the precisions shown in the table are chosen for simplicity.

^bValues given for comparison (Chapter 5).

Table 6.3. Characteristics of the Troposphere^a

	H (km)	N (σ_N) ($10^{-5}s^{-1}$)	L (σ_L) (10^{-3})	l (σ_l) (km)	a (σ_a) (K/km)	Δ_T	Ro_T
O-1	8.513	1329 (7)	247 (7)	1572 (4)	5.2 (0.4)	0.195	0.02
O-10	7.899	1260 (20)	732 (7)	4660 (40)	6.1 (0.6)	0.195	1.91
Os-1	8.001	$10 \cdot 10^2$ ($4 \cdot 10^2$)	$2 \cdot 10^2$ ($1 \cdot 10^2$)	1560 (70)	5 (4)	0.200	0.02
Os-10	7.978	$10 \cdot 10^2$ ($4 \cdot 10^2$)	$8 \cdot 10^2$ ($1 \cdot 10^2$)	5000 (80)	5 (3)	0.122	1.04
Os-360	7.884	$11 \cdot 10^2$ ($5 \cdot 10^2$)	$467 \cdot 10^1$ ($8 \cdot 10^1$)	$297 \cdot 10^2$ ($5 \cdot 10^2$)	5 (4)	0.061	683

Note. — Stratification vs Rotation: H is the scale height, N is the Brunt-Väisälä frequency, L is the normal Rossby deformation radius, l is the Rossby deformation radius, a is the tropospheric lapse rate, Δ_T is the non-dimensional meridional temperature gradient, and Ro_T is the thermal Rossby radius (Section 2.2.3).

^aThe values are restricted to the tropospheric pressure levels of each planet (Figs. 6.5) and 6.6).

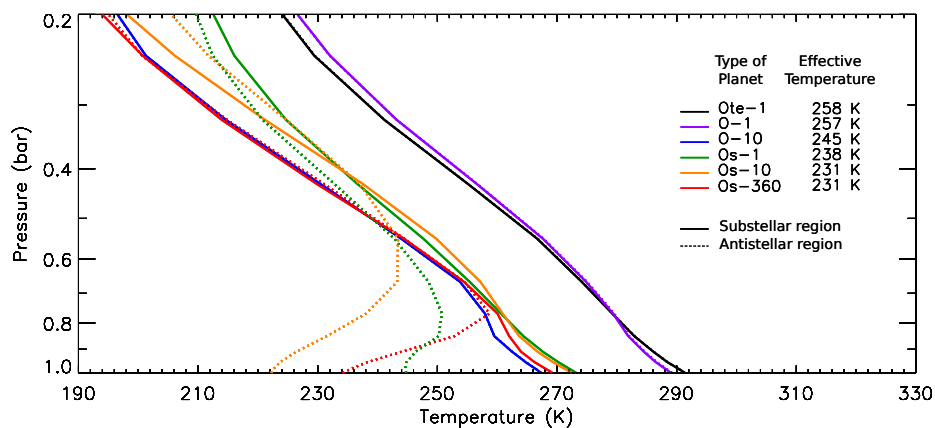


FIGURE 6.1 Atmospheric profiles for the aquaplanets O-1, O-10, O_s-1, O_s-10, O_s-360 (Table 6.1), at the substellar (solid) and antistellar (dotted) regions.

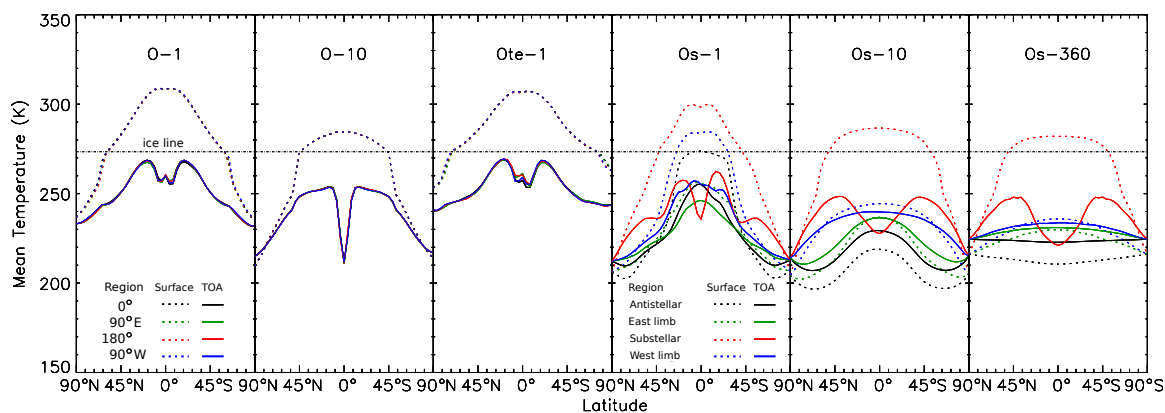


FIGURE 6.2 Mean surface temperature (dashed) and mean brightness temperature (solid) vs latitude for the planets O-1, O-10, O_{te}-1, O_s-1, O_s-10, and O_s-360 (Table 6.1). Colours indicate the sectors where the mean temperature is calculated, each sector has 90° in longitude and is centered on 0° (black), 90°E (green), 180° (red), 90°W (blue), respectively, that in the synchronous planets correspond to the antistellar point, the east (morning) limb, the substellar point, and the west (evening) limb.

As we have explained in Chapter 2, clouds are some of the major players in the energy balance of Earth-like planets through two main effects: First, they increase the planetary albedo as they reflect the incoming radiation at short wavelengths, cooling the planet. This effect depends on the cloud optical thickness, as well as the surface albedo¹. Second, clouds are absorbent in the infrared and for this reason have a direct influence on the greenhouse effect. The most important factor is the difference between the cloud-top temperature – which determines the radiation that will be emitted to space – and the surface temperature, with a large negative difference leading to a warming effect. As the atmospheric temperature generally decreases with height, high clouds have low emission temperatures and a large greenhouse effect – but they can be optically thin in the visible band – while low clouds have a large albedo but a weak greenhouse effect.

The characteristics of the atmospheric circulation of an aquaplanet depend on the rotation speed of the planet. In the tropical zone around the equator, the Coriolis force is weak, and horizontal temperature gradients will be relatively small. The circulation is dominated by thermally direct cells, whose zonally-averaged, meridional components are known on Earth as the Hadley cells. The meridional extent of the Tropics and the Hadley cell are determined by the rotation rate, and to a lesser extent by other parameters such as vertical stability or tropopause height (Hunt, 1979; del Genio & Suozzo, 1987; Frierson et al., 2007). At higher latitudes, the Coriolis force becomes stronger, and the circulation is dominated in both hemispheres by jets in thermal wind balance with larger temperature gradients. Multiple jets can exist in planets with a larger radius.

6.2.1 Non-synchronous aquaplanets

First, in order to study the influence of rotation on aquaplanets, we have built two planets, a case with a rotation rate of one day (O-1), an analogous planet with a

¹In some specific cases, such as above a fresh snow surface, clouds can in fact lightly decrease the planetary albedo

rotation rate of 10 days (O-10), and each one within a circular orbit of a radius of 1 UA and without any obliquity (Table 6.1). O-1 has an atmospheric profile (Fig. 6.1), a surface temperature and an effective temperature (Table 6.2) comparable to the ones of Earth (Ete-1) and of the analogous aquaplanet Ote-1 from the previous chapter. High-latitudes are however colder in O-1, as the lack of obliquity means that the annual-mean insolation is weaker near the poles. The albedo effect of increased sea ice leads to a lower global-mean temperature, and equatorial temperatures that are very close: surface temperatures are comprised between 235 and 309 K in O-1, compared to 253 and 307 K in Ote-1.

The lower rotation rate of O-10 produces an increase in the width of the Hadley cell, that it is represented by the plateau of highest mean surface temperature and the correspondent brightness temperature in Figure 6.2. The meridional temperature gradients are similar in both types of planets (Table 6.2), but the temperature of the slowly rotating planet is lower almost everywhere; these results contradict former studies using simpler models without complete atmospheric physics (Hunt, 1979; del Genio & Suozzo, 1987). The reason seems to be that the dry subsidence region of the Hadley cells is more extended in O-10, leading to a lower greenhouse effect. This initial impact is then increased by feedbacks, including also a larger sea-ice cover than O-1.

Both planets have a narrow region of reduced brightness temperature near the equator, produced by the ITCZ. This brightness minimum is due to a high concentration of high-top convective clouds, clearly apparent in the maps of Figure 6.8. In the case of O-1, the mean surface temperature has a double-peak structure at both sides of the ITCZ, because of a relative temperature minimum in the ocean surface caused by equatorial upwelling (Schopf, 1980; Bakun, 1990; Codron, 2012), where the interaction of easterly trade winds and the ocean by Ekman transport brings cooler deeper water to the surface at the equator and produces a net transport of water to the poles. Equatorial upwelling is absent in O-10, thus the ITCZ has a single peak at the equator. Low clouds are prevalent over the iced surface (Fig. 6.8).

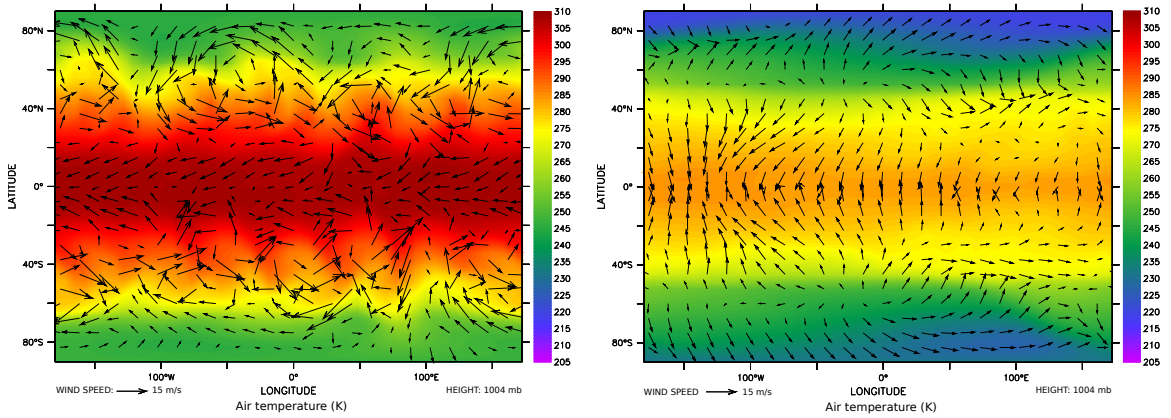


FIGURE 6.3 Mean surface temperature and mean surface wind velocity field in O-1 (left) and O-10 (right).

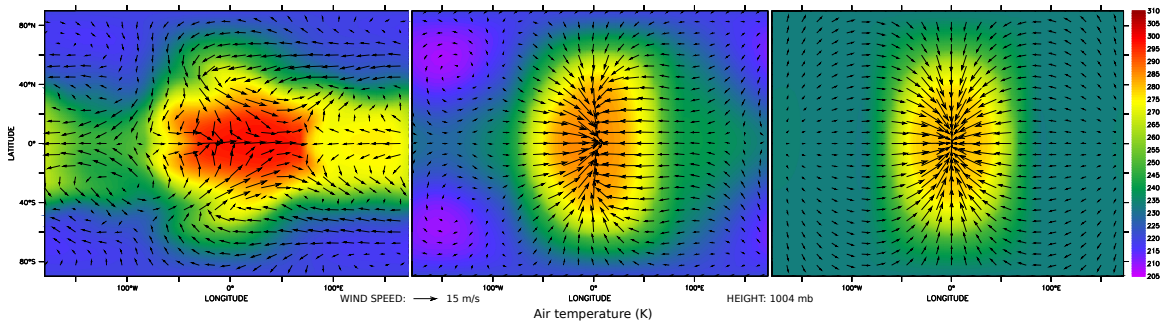


FIGURE 6.4 Mean surface temperature and mean surface wind velocity field for Os-1 (left), Os-10 (center), and Os-360 (right).

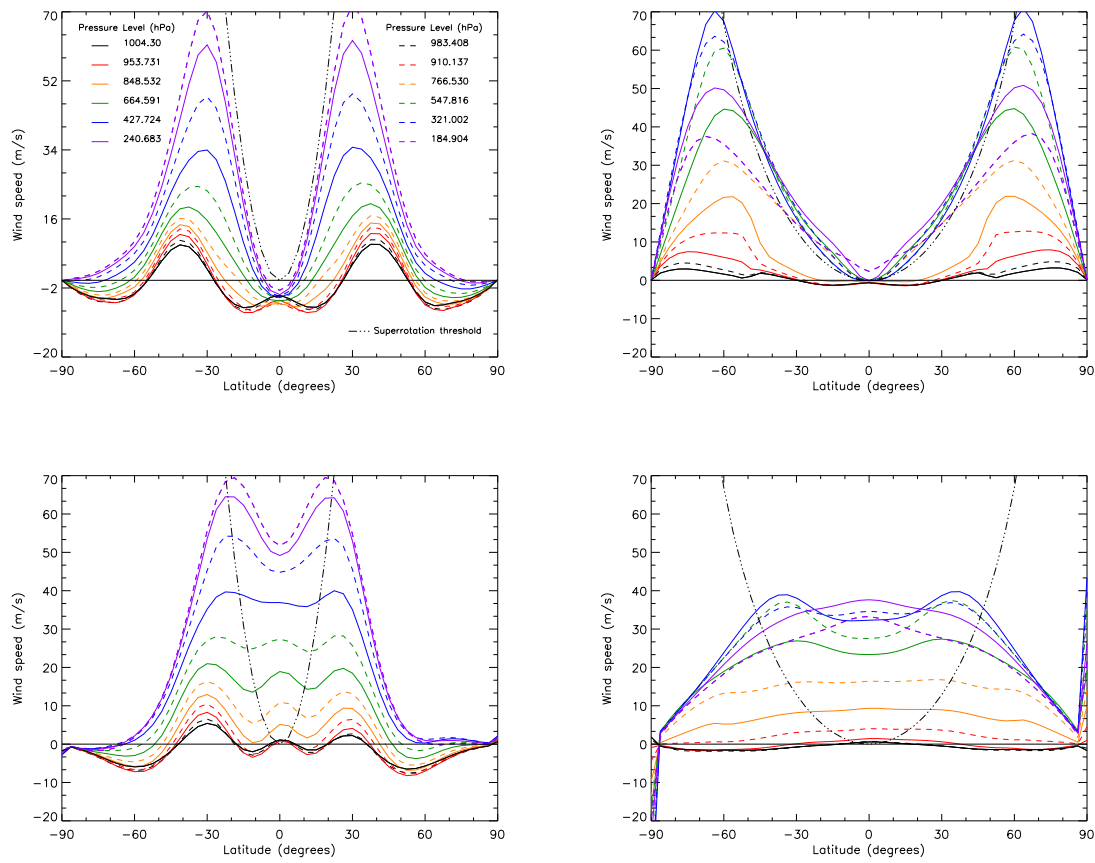


FIGURE 6.5 Mean zonal wind for O-1 (top-left), O-10 (top-right), Os-1 (bottom-left), Os-10 (bottom-right).

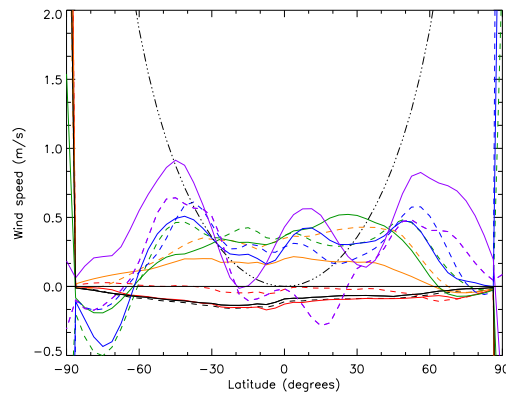


FIGURE 6.6 Mean zonal wind for Os-360.

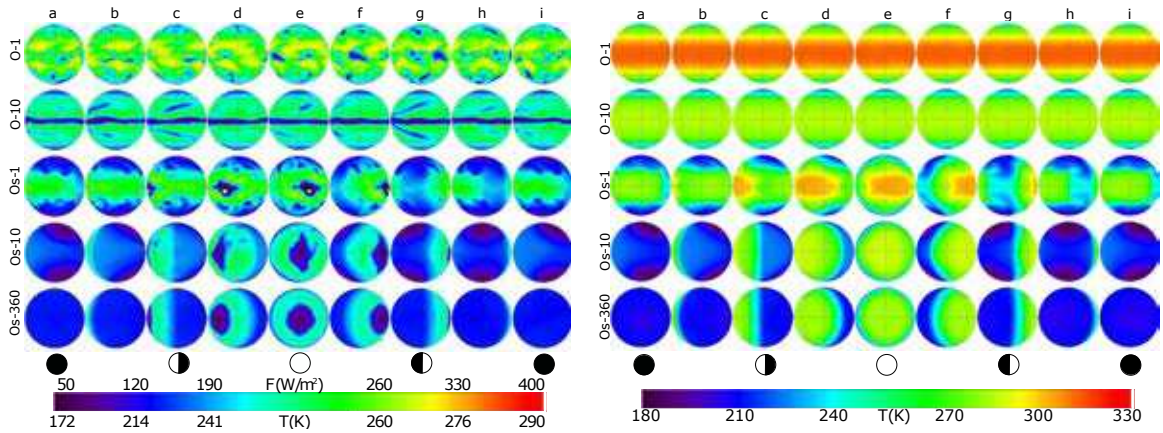


FIGURE 6.7 TOA-all-sky flux (left, scaled in flux and brightness temperature) and surface temperature (right) towards an observer at opposition during one rotation (a-i) for the planets O-1, O-10, Os-1, Os-10, and Os-360. The circles represent the planetary phases of the tidally-locked planets for an observer at the equator.

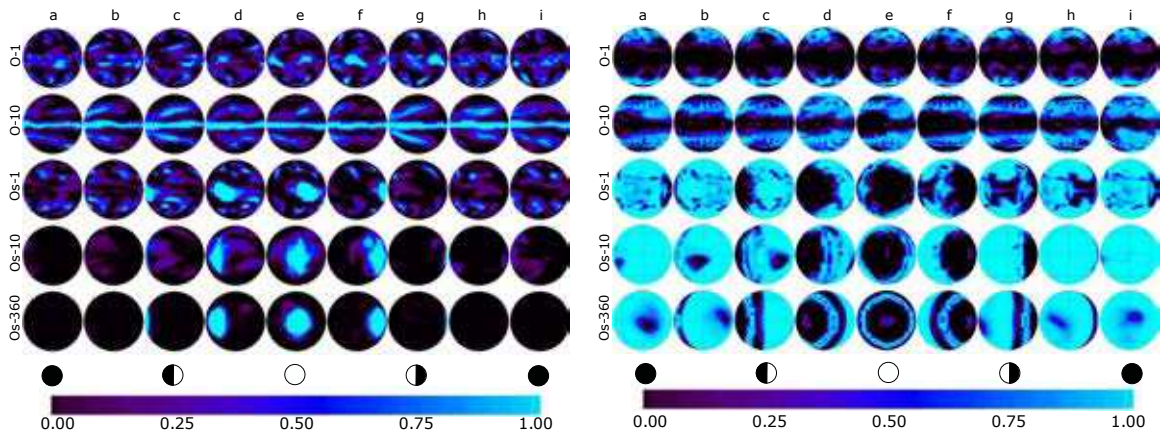


FIGURE 6.8 High cloud fraction (left) and low cloud fraction (right) towards an observer at opposition during one rotation (a-i) for the planets O-1, O-10, Os-1, Os-10, and Os-360. The circles represent the planetary phases of the tidally-locked planets for an observer at the equator.

The day/night temperature contrast is negligible, as can be seen in Figure 6.7 and in Figure 6.2, where the curves are almost coincidental for every point of view. This is due to the high thermal inertia of the surface, whether the 50-m ocean mixed layer or the sea ice layer (as both the thermal inertia of sea-ice and the diurnal cycle of absorbed shortwave radiation are weak).

Figure 6.3 shows the annual mean surface temperature and wind field for O–1 (left) and O–10 (right). The equatorial zonal wind and the instability regions ($\sim 40^\circ$ latitude) in O–1 are clearly seen, in O–10 the zonal wind is weak and there is a region of convergence in the form of a “chevron”². The winds are predominantly meridional near the equator, where the Coriolis force is minimum, and zonal near the poles, the chevron is orientated south-west to north-east in the Northern Hemisphere and south-east to north-west in the Southern Hemisphere. As in any region of convergence, convection clouds are formed, giving the characteristic pattern of Figure 6.7. Figure 6.5 show that the mean zonal wind speed per latitude and the superrotation limit (dot-dash line). O–10 shows equatorial superrotation in the upper troposphere, it extends to a latitude range of 40° at $\sim 767 \text{ hPa}$, to a 60° at $\sim 185 \text{ hPa}$. The “chevron” cloud opens at high latitudes because the superrotation wind speed increases with latitude. As in the case of Ete–10 (Figure 5.14), the superrotation is faint, however wind speeds are higher in aquaplanet analogues than in planets with continents because the friction of the wind with water is lower than the friction with land.

6.2.2 Synchronous aquaplanets

The atmospheric circulation of tidally-locked planets is rather symmetric respect to the substellar point, because its permanent position. In order to separate insolation regimes, in Figure 6.2, we have pictured the mean surface temperature along with

²A similar pattern has been observed in slow planets with superrotation winds as Titan and Venus, but curiously, the orientation of the chevron is the opposite, with the tip pointing eastwards. The origin of this arrow is the combination of Rossby and Kelvin waves, (Tokano, 2011; Showman & Polvani, 2011)

the brightness temperature within different sectors of the planet, each covering 90° in latitude: q1 is centered at 0° longitude in the center of the nightside, q3 at the substellar point, q2 at 90°W and q4 at 90°E at terminators.

In tidally-locked planets, the ITCZ is replaced by a region of ascending air around the substellar point, largely covered by high clouds that result in a pronounced minimum in brightness temperature as it is also visible on the maps of Figure 6.7 and Figure 6.8. Then the circulation transports heat away from the permanent dayside, preventing an atmospheric collapse on the nightside. This transport is more efficient above the surface boundary layer, leading to temperature inversion on the nightside (Figure 6.1), which helps the formation of low cloud decks (Figure 6.8).

At the same time, the high albedos of the low clouds and the ice, which cover a large part of the surface away from the substellar point, strengthen this effect (Figure 6.2), and mean surface temperatures on the planet are between 300 and 210 K. Merlis & Schneider (2010), with a model with simplified physics, obtains warmer temperatures (300 K- 250 K), possibly because of the weak greenhouse effect or the albedo of the high clouds in the substellar region. The ice-albedo feedback is likely to be weak however, as the ice-covered regions are the ones receiving little insolation (Joshi et al., 1997). The heat transport by the ocean is limited to the ice-free region.

The actual dynamics of the atmosphere depends on the rotation rate. In the slowly rotating planet (Os-360), the circulation is symmetric with respect to the substellar point (del Genio & Zhou, 1996). In the rapidly rotating planet (Os-1), the zonal asymmetry in insolation creates stationary Rossby and Kelvin waves that carry momentum towards the equator and generate the equatorial superrotation (Merlis & Schneider, 2010; Showman & Polvani, 2011). The tropical jet is strong enough to shift eastward the position of the minimum and maximum of temperature by ~ 90 degrees and ~ 20 degrees respectively. The rapid rotation also limits poleward heat transport by a thermally direct cell, leading to a larger meridional temperature gradient (see

Table 6.2). The intermediate rotation rate (Os-10) resembles the slow

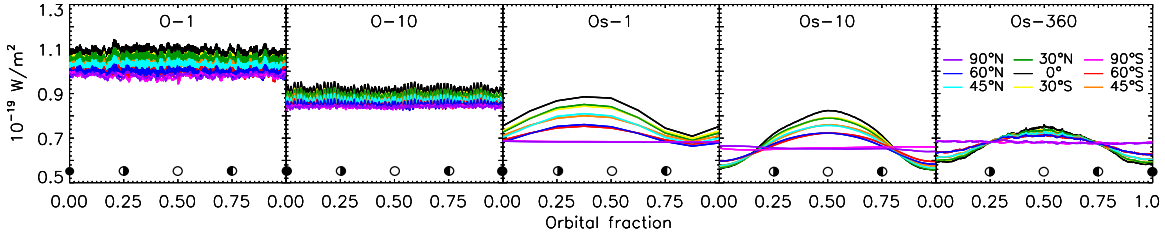


FIGURE 6.9 TOA-all-sky flux orbital series for the terrestrial planets O-1, O-10, Os-1, Os-10, and Os-360. The circles represent the planetary phases of for an observer at the equator.

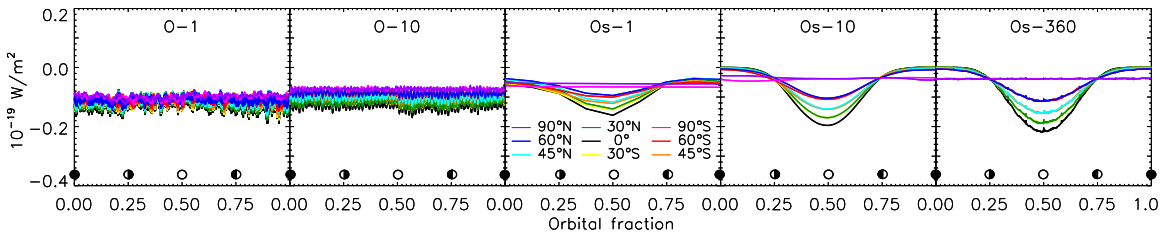


FIGURE 6.10 Cloud Radiative Forcing corresponding the orbital series for the terrestrial planets O-1, O-10, Os-1, Os-10, and Os-360. The circles represent the planetary phases of for an observer at the equator.

case, with similar circulation patterns, albedos, greenhouse parameters, and surface and effective temperatures. But the rotation of Os-10 still leads to anisotropy, shown as the temperature minimum at $\sim 60^\circ$ latitude in both hemispheres (Figure 6.2, Figure 6.4 and Figure 6.7). It is remarkable that especially for Os-1 and also for Os-10, the minimum temperatures are not found near the antistellar point but near the poles. Figure 6.4, which represents the mean temperatures and the wind velocity fields at the surface of the set of synchronous planets, shows that the winds always converge in the warmest region of the planet.

In Figure 6.5 and Figure 6.6 we see that there are superrotating winds in the three

Table 6.4. Time series variability

	Variability	Orbital phase	Latitude								
			90	60	45	30	0	-30	-45	-60	-90
Ete-1 ^a	Rotational	[4/12,5/12]	3	4(5)	5(6)	5(7)	4(6)	4(5)	4(5)	3(4)	2
	Orbital	[0-1]	19	17(15)	14(12)	11(9)	5(3)	4(6)	6(8)	8(9)	10
Ote-1 ^a	Rotational	[4/12,5/12]	2	4(4)	5(5)	6(6)	6(7)	6(7)	5(6)	4(5)	2
	Orbital	[0-1]	8	8(6)	8(5)	7(3)	5(4)	5(7)	6(8)	8(9)	9
O-1	Rotational	[0,1/12]	2	4	5	6	6	6	5	4	2
	Orbital	[0-1]	2	3	3	3	3	3	3	3	2
O-10	Rotational	[0,1/12]	2	3	4	5	5	5	4	3	2
	Orbital	[0-1]	1	2	2	2	2	2	2	2	1
Os-1	Orbital	[0-1]	2	12	16	18	19	17	14	11	2
Os-10	Orbital	[0-1]	3	15	21	25	28	25	21	16	3
Os-360	Orbital	[0-1]	2	13	17	20	24	20	17	12	2

Note. — Time series variability for aquaplanets O-1, O-10, Os-1, Os-10, Os-360. Values as percentage over the mean.

^aValues given for comparison (Chapter 5).

planets. The superrotation band extends to $\sim 30^\circ$ in latitude in Os-1, that shows winds speeds values similar to the Earth, with a maximum speed of ~ 70 m/s. Os-10 has a superrotation winds within a band that extends to $\sim 45^\circ$, the with maximum speed (~ 40 m/s) is lower to to the colder temperatures and the slower rotation of the planet. On the contrary, the state of Os-360 is stable and the net circulation is negligible with speeds < 1 m/s. Figure 6.7 and Figure 6.8 shows the symmetry respect to the substellar point as well as the surface of ice and water, the cloud covering, and the heat transport along of the planet for an observer at opposition at the equatorial plane.

6.3 Time series analysis

Figure 6.9 illustrates the orbital thermal light curves of the planets at a distance of 10 pc, for nine different observer's inclinations. As it was previously explained, the

TOA emission is perturbed by the presence of high clouds. We have also calculated the correspondent CRF, at each point of the series in order to quantify the relevance of this absorption on the integrated signal (Figure 6.10).

6.3.1 Non-synchronous aquaplanets

The planetary thermal emission is essentially dependent on insolation, for this reason the light curves of O-1 and O-10 depend on the observers position. Rotation rate and the high thermal inertia of water prevent from having significant differences between day and night, and in the absence of seasons, the variability is strictly produced by the presence of high clouds. In non-synchronous aquaplanets, the production of this type of clouds is determined by the atmospheric circulation and not by illumination, as it is the case of terrestrial planets (Chapter 5). Low clouds are more abundant near the poles over the permanent ice caps (Figure 6.8), whereas at low latitudes, warm convective currents rise the clouds to higher levels of the troposphere. For this reason high clouds are mainly placed along the ITCZ.

As expected, in O-1, the rotational variability of the planet (Table 6.4) is comparable to an aquaplanet with the axial tilt of the Earth (Ete-1), whereas it has a little orbital variability, as it is just produced by the fluctuation of clouds.

In O-10, the atmosphere is colder and less turbulent than in O-1 and the clouds are evenly distributed along the ITCZ. High clouds also appear along the mid-latitude convergent region producing a “chevron” cloud pattern (Merlis & Schneider, 2010; Showman & Polvani, 2011). The cyclical appearance of this pattern causes an additional frequency modulation on the signal of the planet.

6.3.2 Synchronous aquaplanets

In planets with circular orbits, the thermal light curve of tidally locked planets gives an important information about the distribution of the brightness temperature on the planet. The maximum and the minimum of the curve correspond respectively

to the permanent day and night sides of the planet. However, because of the atmospheric circulation, these features can be shifted from the substellar and the antistellar points by several degrees (e.g., Fortney et al., 2006; Knutson et al., 2007), a fact that is useful to distinguish between atmospheric and airless planets (Seager & Deming, 2009).

The atmosphere has a large CRF near the substellar point, where the tropospheric wind converges forming a huge condensation cloud (Figure 6.4 and Figure 6.8). The nightside can be colder and drier than the poles. However, in Os-1, the superrotation jet warms the nightside, displacing the minimum of temperature to lower latitudes ($\sim 60^\circ$). Then, although the polar views have the lowest brightness temperature, the minimum value of the orbital series belongs to views at $\sim 60^\circ$ in latitude (Figure 6.9), because of the circulation and the thermal inertia of the atmosphere. The maximum is shifted 15°E (Table 6.2 and Figure 6.9). In the case of Os-10, this shift is barely appreciated in the light curve because, although slower planets have lower temperatures, the atmosphere is less turbulent and as a consequence the CRF is larger at the substellar point (Fig. 6.7 and Fig. 6.10), absorbing the thermal emission from below. This extreme difference between the dayside and the nightside is represented by the orbital variability (Table 6.4).

It is interesting to note that in Os-1, the variability at the equator is comparable to the seasonal change at Earth's north polar view. For tidally-locked planets with slower rotation rates the variability increases, but it is not directly proportional as it also depends on the climate, specially on the extension of the iced surface and the magnitude of the convective clouds over the warmest point of the planet.

6.3.3 Parameters retrieved from the series

As we have shown in Section 2.2, the planetary effective temperature and albedo can be retrieved from the orbital light curves. Table 6.5 shows the results for nine different positions of the observer. High latitudes, being colder and more abundant

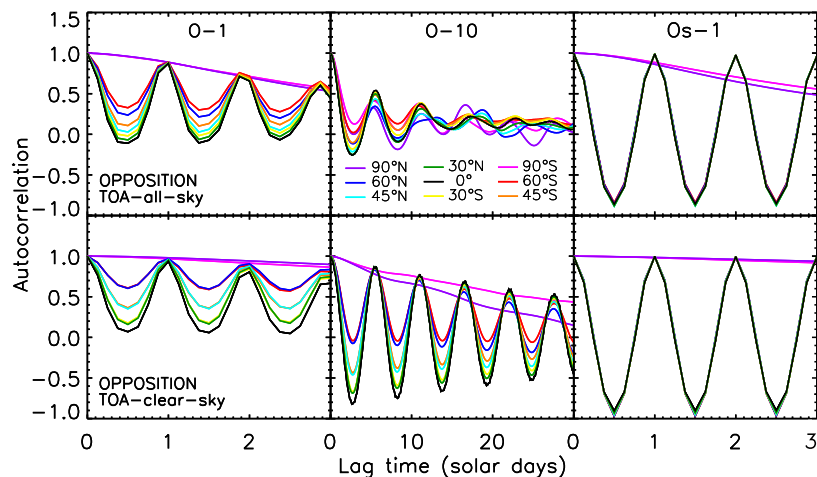


FIGURE 6.11 TOA-all-sky autocorrelation series for an observer at opposition for the planets O-1, O-10, and Os-1.

in low clouds, present higher albedos and lower effective temperatures, whereas observers over low latitudes, where the insolation is higher, retrieve higher effective temperatures and lower albedos. For every planet, latitudes $\sim 30^\circ$ give results near to the global value.

6.4 Periodicities

We have used the autocorrelation analysis of the time series to obtain the rotation period of the five planets (Section 2.3). As the rotation period of tidally-locked planets can be directly retrieved from their thermal orbital light curve, in this section, we only present the results for O-1 and O-10 (Figure 6.10 and Table 6.5).

Figure 6.11 give the autocorrelation for the TOA-all-sky emission (top) and the TOA-clear-sky emission (bottom). The latter also contains the information of humidity, without the cloud absorption, for this matter, the period obtained is given by the distribution of the humidity related to convective regions (1 day for O-1 and ~ 6 days for O-10). The TOA-all-sky emission shows the effect of the cloud absorption.

Table 6.5. Observed parameters^a

		Global Value	Latitude								
			90	60	45	30	0	-30	-45	-60	-90
O-1	T_{eff} (K)	257	253	254	256	257	259	257	256	254	253
	Albedo	0.27	0.32	0.31	0.29	0.27	0.25	0.27	0.29	0.31	0.32
	\mathcal{T} (days)	0.99	-	1.00	1.00	1.00	1.00	1.00	1.00	1.00	1.00
O-10	T_{eff} (K)	245	243	243	244	245	246	245	244	243	243
	Albedo	0.40	0.41	0.42	0.41	0.40	0.39	0.40	0.41	0.42	0.41
	\mathcal{T} (days)	9.97	-	10.75	6.25	6.25	6.25	6.25	6.25	6.25	10.75
Os-1	T_{eff} (K)	238	231	234	237	239	241	239	237	234	232
	Albedo	0.46	0.52	0.50	0.48	0.46	0.44	0.45	0.48	0.50	0.52
	\mathcal{T} (days)	1.00	-	1.00	1.00	1.00	1.00	1.00	1.00	1.00	1.00
Os-10	T_{eff} (K)	231	229	229	230	231	232	231	230	230	229
	Albedo	0.52	0.54	0.54	0.53	0.52	0.51	0.52	0.53	0.54	0.54
	\mathcal{T} (days)	10.00	-	10.00	10.00	10.00	10.00	10.00	10.00	10.00	10.00
Os-360	T_{eff} (K)	231	231	231	231	230	230	230	231	231	231
	Albedo	0.53	0.52	0.53	0.53	0.53	0.53	0.53	0.53	0.53	0.53
	\mathcal{T} (days)	360.0	-	360.0	360.0	360.0	360.0	360.0	360.0	360.0	360.0

^aObserved parameters from the time series: effective temperature T_{eff} , albedo A and rotational period \mathcal{T} (Chapter 2) for the planets Ete-1, Ete-10, Ote-1, and SOte-1 at opposition and at conjunction (in parentheses) for several sub-observer's point latitudes. Values are calculated as the percentage over the mean value.

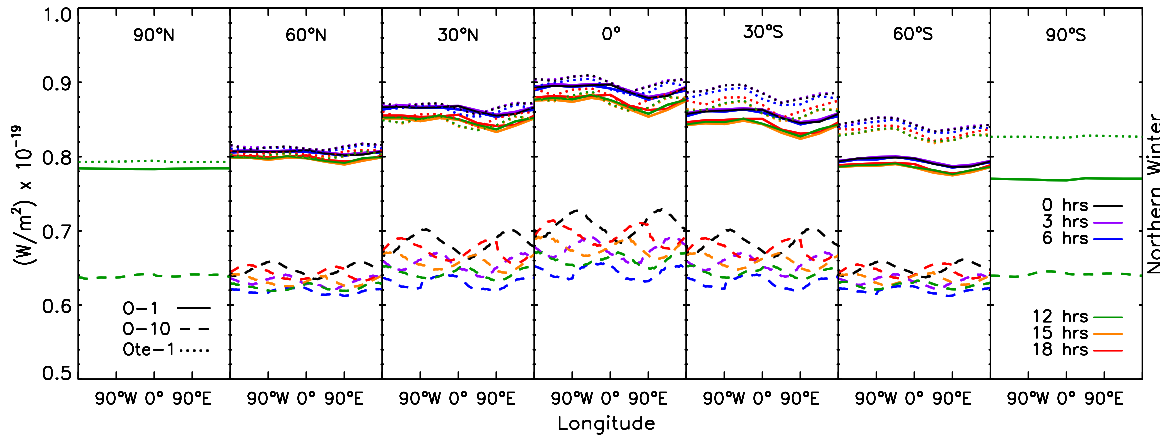


FIGURE 6.12 Rotational series for the planets O-1 and O-10. Ote-1 rotational series during northern winter is given for comparison. Colors represent the local hour at the planetary disk center meridian.

Table 6.5 shows a dispersion in the rotation rates of O-10 with latitude, due to the superrotation of the atmosphere.

To set an example, due to the day/night contrast and the steady state of the weather patterns, the autocorrelation of Os-1 clearly shows a rotational period of 1 day for every observer (except for polar ones where the planetary view does not change). However, in the case of non-synchronous aquaplanets with circular orbits, the variability of the signal comes only from the presence of clouds. When the rotation period is longer than the cloud lifetimes, as in O-1, the autocorrelation is reinforced. On the contrary when the cloud lifetimes are shorter than the planetary rotation, as in O-10 due to the superrotation of the atmosphere, the regions are periodical but the clouds change after one rotation of the planet, and then the autocorrelation obtained by a distant observer, becomes worse with time.

6.5 Average rotation light curves

As in Chapter 4, we can build an average daily signal by time-folding the series with the value of the rotation period obtained by autocorrelation. This method

minimizes the fluctuations of the signal and the steady features stand out. It is useful to compare Figure 6.12 with Figure 6.7 and Figure 6.8. Whereas Figure 6.7 and Figure 6.8 represent the planetary disk seen by an equatorial observer at opposition during one rotation, Figure 6.12 shows the rotational average series for O–1, O–10 and Ote–1 (Chapter 5). Each graph of Figure 6.12 is formed by the views of the planet at the same local hour (each view of Figure 6.7 correspond to the graphs at 0 hrs). Following this description, these type of curves are observed by a unique observer only in the case of planets with circular orbits and without axial tilt, as it are the cases of O–1 and O–10. In the absence of seasons, the planet receives the same energy at every point of the orbit and the short rotation period allow the observer to built the graphs of Figure 6.12.

As expected, O–1 does not present significant variabilities within one period and resembles the average rotation curve of Ote–1, with the exception that the latter, having an axil tilt, has a change in the mean temperature level produced by the seasons and the southern hemisphere is warmer due to the eccentricity of the orbit.

Taking in account the superrotation of the atmosphere, the clouds of O–10 exhibit a diurnal cycle. The planet gets warmer during the day, the absorbtion of the convective clouds becomes stronger, the “chevron” pattern appears at both the substellar and the antistellar point at afternoon (15 hr, local), moves towards the east (as it rotates faster than the solid body). It grows being maximal at midnight (0 hr, local). Then, it rains during the night then the cycle starts again at 15 hr.

6.6 Summary

In this chapter, we have studied the thermal emission of five aquaplanets with circular orbits and without axial tilt (without seasons): O–1 and O–10 have a rotation rate of 1 and 10 days, respectively; and three synchronous aquaplanets Os–1, Os–10, Os–360 with rotation rates of 1, 10 and 360 days, where the stellar constant is modified according to the orbital distance.

Aquaplanets analogues are warmer than terrestrial planets, with an ITCZ with a high concentration of convective clouds because the large specific humidity. An aquaplanet with the same orbital parameters than the Earth has an effective temperature of 258 K , an aquaplanet analogue with a circular orbit and without axial tilt, has an effective temperature of 257 K . Synchronous aquaplanets however have low surface temperatures and the main part of the surface is frozen except for the antistellar region, an Earth analogue with a rotation rate of 1 day, has an effective temperature of 238 K . The warmest point is usually shifted by the circulation of the planet and being a convergence region, steady convection clouds cover the area, which has a slight effect over the signal by decreasing the TOA-emission at this point.

Because of the low thermal inertia of water, the cloud absorption is the only source of flux variability in the signal. Thus, the period is retrieved by autocorrelation if the cloud lifetimes are longer than the period of the planet or if the clouds are linked to convergence regions. Thus, the period is retrieved in O-1 because the rotation rate is shorter than the clouds lifetimes. O-10 has a convergence region in the form of a “chevron” pattern, however the region is an atmospheric phenomenon and it is not linked to surface steady features. The period obtained is shorter than the period of rotation of the planetary surface, because the equatorial superrotating winds in the upper troposphere drive the clouds of the “chevron” pattern. The “chevron” cloud opens at high latitudes because the superrotation wind speed increases with latitude. The movement of the “chevron” pattern is shown in longitudinal light curves. The period of tidally locked planets is retrieved because the convergence regions are tied to the surface temperature maximum.